



Highly sensitive surface-enhanced Raman scattering (SERS) imaging for phenotypic diagnosis and therapeutic evaluation of breast cancer

Chonggui Qiu^{a,b,1}, Wei Zhang^{a,b,1}, Yanhong Zhou^{a,b,1}, Hongwang Cui^a, Yanlong Xing^{a,b}, Fabiao Yu^{a,b,*}, Rui Wang^{a,b,*}

^a Key Laboratory of Hainan Trauma and Disaster Rescue, The First Affiliated Hospital of Hainan Medical University, Hainan Medical University, Haikou 571199, China

^b Engineering Research Center for Hainan Bio-Smart Materials and Bio-Medical Devices, Key Laboratory of Emergency and Trauma, Ministry of Education, Key Laboratory of Hainan Functional Materials and Molecular Imaging, College of Pharmacy, College of Emergency and Trauma, Hainan Medical University, Haikou 571199, China

ARTICLE INFO

Keywords:

Surface-enhanced Raman scattering (SERS) imaging
Phenotypic biomarker detection
Breast cancer
Chemotherapy and surgery
Therapeutic evaluation

ABSTRACT

The invasion and metastasis of breast cancer are closely related to various biomarkers expressed on the surface of tumor cells and the tumor microenvironment. The deficiency of sensitive phenotypic diagnosis and therapeutic evaluation toward breast cancers represents a significant challenge in cancer diagnosis and therapy. Herein, we report a crucial example of surface-enhanced Raman scattering (SERS)-based imaging utilizing highly sensitive SERS probes to serve as a robust platform for the detection of breast cancer phenotypic biomarkers expressed on the cell surfaces and therapeutic evaluation after chemical therapy and surgery. The SERS probes feature gold-silver (Au@Ag) core-shell nanoparticles with double-layer Raman reporters embedding on the surfaces of the gold core and silver shell, respectively, which further conjugate with specific antibodies. The highly enhanced SERS signals permit the sensitive detection of specific phenotypic biomarkers expressed on the cell surface. In the present work, the epidermal growth factor receptors (EGFR and ErbB2) and insulin-like growth factor 1 (IGF1) were selected as the target biomarkers and assessed the expression in MCF-10A human normal breast cell line and MDA-MB-468, SK-BR-3, KPL-4 human breast cancer cell lines through the SERS-based imaging technique. In the xenotransplanted breast tumor model, systematic delivery of SERS probes enabled precise therapeutic evaluation after anticancer drug tamoxifen therapy and surgery treatment through SERS imaging. Consequently, SERS imaging was consistent with H&E and Masson staining. These results suggest the proposed SERS-based imaging technique has a strong potential to be a powerful tool for precise diagnosis and therapeutic efficacy of breast cancers.

1. Introduction

Breast cancer becomes the most common cause of cancer deaths in women worldwide. More than 570,000 people die of the disease only in China and USA in 2021 [1]. The breast cancer is highly heterogeneous, and its biological behavior with the same pathological grade is also different [2,3]. Simultaneously, its invasion and metastasis are closely related to the various biomarkers expressed on tumor cells and the tumor microenvironment. Even breast cancers with the same type, grade and stage show completely different treatment responses and prognosis due to differences in their molecular phenotypes [4,5]. Nowadays, the

breast cancer classification based on the dominance principle has certain limitations in reflecting tumor histological characteristics, biological behavior and prognosis, and cannot meet the requirement of precise tumor diagnosis and refinement in personalized treatment [6]. Therefore, it is an urgent need to develop a new type of tumor typing and diagnosis technology for the detection of tumor molecular phenotype.

At present, the pathological tissue section test is the "gold standard" for diagnosing breast cancer [7]. Unfortunately, due to the differences in the morphology of tumor sections under the microscope and the influence of pathologists' subjective judgments, certain errors are inevitably caused. Moreover, the acquisition of pathological sections needs to

* Corresponding authors at: Key Laboratory of Hainan Trauma and Disaster Rescue, The First Affiliated Hospital of Hainan Medical University, Hainan Medical University, Haikou 571199, China.

E-mail addresses: yufabiao@hainmc.edu.cn (F. Yu), wangrui@hainmc.edu.cn (R. Wang).

¹ These authors contributed equally to this work.

penetrate deep into the lesion tissue, which is likely to cause certain trauma. Therefore, the development of non-invasive breast cancer imaging technology has gained increasing attention for the early and accurate diagnosis of breast cancer. Recently, commonly clinical imaging techniques, including X-ray mammography, ultrasound, computed tomography (CT) and magnetic resonance imaging (MRI), are used to observe lesions based on changes in tumor anatomy [8,9]. However, the traditional imaging techniques have obvious limitations in the accurate diagnosis and detection of micrometastases (tumor lesions > 1 cm). Optical imaging as a powerful alternative to the above imaging technologies has attracted more and more attentions, which is based on targeted optical probes and can detect tumor cell abnormalities at an early stage, even at the molecular level [10–12]. Accurate diagnosis and individualized treatment of breast cancer are the keys to improving patient survival. Now, the main treatment methods for breast cancer are surgery, radiotherapy, and chemotherapy. Accurately assessing the treatment efficacy is of great significance for improving patient survival.

Surface-enhanced Raman scattering (SERS) technique for biomedical imaging is gaining sustained interest due to its ultrahigh sensitivity, negligible auto fluorescence, multiplexed detection capability, and resistance to photobleaching compared to other imaging techniques (fluorescence, MRI, and ultrasound) [13–15]. The SERS imaging can specially make a distinction between SERS probe-contained tumors and surrounding normal tissues through the fingerprint signals of Raman reporter molecules [16]. The Raman signals of reporter molecules can be significantly enhanced by active SERS substrates, which is beneficial to sensitive tumor diagnosis with ultralow limits of detection [17–19]. Previous research works on SERS imaging often focus on solid tumor detection, while very few investigations illustrate its applications in simultaneous phenotypic biomarker detection and therapeutic evaluation [20–25]. To overcome the obstacle, SERS probes are desired to meet the following criteria: (i) ultrahigh sensitivity for tumor detection, even few microtumor cells; (ii) high specificity for different phenotypic biomarkers in different cell types; (iii) excellent chemical- and photostability to avoid the biological degradation and maintain the SERS signals in the complex tumor microenvironment even after the long-time systematic circulation. To the best of our knowledge, there are still challenges to meet all the criteria.

Herein, we explore SERS probes capable of achieving precise diagnosis and accurate therapeutic evaluation of breast cancer through the detection of growth factor reporters on tumor cell membranes. The SERS probes are made of Au@Ag core-shell nanoparticles, decorated with Raman reporter double-layer on the surface of Au core and Ag shell with functional polyethylene glycol (HS-PEG-NHS) layer for the antibody conjugation [26,27]. The design of a double-layer Raman reporters creates significantly enhanced Raman signals for ultrahigh sensitivity, thus contributing to mapping tumor cells with high contrast. Furthermore, after equipping the specific antibodies for growth factor reporters, the SERS probes can actively target the tumor cells for precise detection of phenotypic biomarkers and therapeutic evaluation. With all these features, we prepare xenotransplanted breast tumor models and delineate systematic delivery of SERS probes for therapeutic evaluation after tamoxifen treatment and removing the bulk solid tumors through surgery. We expect this study would broaden the application of SERS imaging toward precise diagnosis and non-invasive evaluation of breast cancer.

2. Experimental section

2.1. Materials and instruments

Gold (III) chloride trihydrate ($\text{HAuCl}_4 \cdot 3\text{H}_2\text{O}$) and mercaptopolyethylene glycol-succinimidyl ester (HS-PEG-NHS, MW = 3000) were purchased from Sigma-Aldrich (St Louis, MO, USA). Malachite green isothiocyanate (MGITC), rhodamine B 5-isothiocyanate (RBITC) and 3, 3'-diethylthiatri carbocyanine iodide (DTDC) were purchased

from Invitrogen (Carlsbad, CA, USA). Rabbit anti-EGFR monoclonal antibody (ab52894), rabbit anti-IGF1 monoclonal antibody (ab182408) and rabbit anti-ErbB2 monoclonal antibody were purchased from Abcam (Shanghai, China). The ultrapure water ($18 \text{ M}\Omega \cdot \text{cm}^{-1}$) used in this study was prepared by a Milli-Q water purification system (Billerica, MA, USA). All the other reagents were from commercial sources with analytical reagent grade and used without any further purification.

The UV-vis absorption spectra were obtained using an FL-QM spectrophotometer (Horiba, Japan). Dynamic light scattering (DLS) data were collected from an SZ-100Z2 particle size analyzer (Horiba, Japan). Transmission electron microscopy (TEM) images were gained through an HT7800 (Hitachi, Japan) instrument at an accelerating voltage of 120 kV. Raman measurements were obtained using Renishaw inVia Qontor Raman microscope system (Renishaw, UK).

2.2. Synthesis of gold nanoparticles

Gold nanoparticles (AuNPs) were prepared based on the previously reported seed growth method [28]. All glassware was washed in aqua regia, then rinsed with ultrapure water and dried before use. 75 mL of 2.2 mM sodium citrate solution was stirred and heated to boiling, then, 0.5 mL of 25 mM HAuCl_4 solution was added to prepare the seed nanoparticles. When the temperature of the gold seed solution was cooled to 90 °C, 0.5 mL of 60 mM sodium citrate solution and 0.5 mL of 25 mM HAuCl_4 solution were added, and the addition was repeated twelve times at two-minute intervals. The temperature was kept at 90 °C, and the color of the solution changed from bright red to wine red as the number of additions of sodium citrate and HAuCl_4 solution increased. After stirring at 90 °C for 30 min, the solution was cooled to room temperature to obtain AuNPs. The shape and size distribution of AuNPs were characterized by DLS and TEM.

2.3. Synthesis of Au@Ag core-shell NPs

Au@Ag core-shell NPs were synthesized via the reduction of silver nitrate (AgNO_3) by ascorbic acid (AA). Under vigorous stirring, 10 mM ascorbic acid was firstly added to 5 mL of AuNPs, and 10 mM silver nitrate was dropped into the above mixture. After reacting for 1 h, the Au@Ag core-shell NPs could be obtained. The silver thickness could be adjusted by changing the volumes of silver nitrate and ascorbic acid. The properties of Au@Ag core-shell NPs were studied through UV-vis, DLS, TEM and SERS.

2.4. Synthesis of SERS probes

The SERS probes were prepared according to our previous research with minor modification. 0.5 μL of MGITC solution (10^{-2} M) was added to 1 mL of AuNPs. After shaking for 30 min, 10 mM ascorbic acid solution and 10 mM silver nitrate solution were added. After stirring for 1 h, 0.5 μL of MGITC solution (10^{-2} M) was added and reacted for another 30 min to modify the second MGITC layer on the surface of the Ag shell.

To activate the -COOH group of the antibodies for conjugation with HS-PEG-NHS, EDC solution in ice water was introduced into HS-PEG-NHS with the same molar mass. After shaking for 30 min at 4 °C, the antibodies with the same molar mass were added and shaken overnight at 4 °C. To conjugate the HS-PEG-antibody onto the surface of nanoparticles, the Au@Ag core-shell NPs were redispersed in Na_2CO_3 aqueous solution (1.04 μM , pH 8–9). Then, HS-PEG-antibody was added to the Au@Ag core-shell NPs and reacted for 2 h, then 10 % BSA was added. After 1 h, excess BSA was removed through centrifugation (7000 rpm, 30 min) and resuspended in PBS (50 mM, pH 7.4).

2.5. Cell culture

Human normal mammary epithelial cell line (MCF-10A) and human breast cancer cell lines (KPL-4, SK-BR-3, and MDA-MB-468) were from

Procell in Wuhan, China. MCF-10A, KPL-4, SK-BR-3, and MDA-MB-468 cells were incubated in MCF-10A special medium, L-15 medium, McCoy's5A medium and high glucose DMEM medium supplemented with 10 % FBS and 1 % antibiotics (penicillin/streptomycin, 100 U/mL), respectively. All the cells were cultured at 37 °C in a 95 % humidified atmosphere with 5 % CO₂.

2.6. Cytotoxicity of SERS probes

The cytotoxicity of the SERS probes was tested by the CCK-8 assay. The cells (5×10^3 cells/cell in 96-well plate) were incubated for 24 h at 37 °C under 5 % CO₂, then different concentrations of SERS probes (0, 1, 2, 5, 10 nM) were added. After incubation for 24 h under the same conditions, the cells were washed twice with PBS and CCK-8 solution was added to the wells for further incubation. Then the optical density (OD) was measured at 450 nm using a microplate reader (BioTek, USA). When the amount of the probe added was 0 nM, the cell viability value was set to 100 %. The cell viability was calculated by the use of the equations shown below.

$$\text{Cell viability(\%)} = (\text{Mean OD of sample} \times 100) / (\text{Mean OD of the control group}).$$

2.7. Cell imaging

The cells were seeded on confocal cell culture dishes for 24 h and then incubated with 10 nM of 10 μL SERS probes. Subsequently, cells were washed with PBS three times and fixed using 4 % paraformaldehyde for 15 min. The fixed cells were washed twice using deionized water and air-dried. SERS imaging of cells was performed with a 633 nm laser and 1 s exposure time (1 μm step size, 100 × objective, 20–25 min imaging time).

2.8. In vitro detection limit of SERS probes

The agarose phantoms containing SERS probes were utilized to test the detection limit of SERS probes. Briefly, the warm liquid agarose was mixed with different concentrations of SERS probes at 0, 1, 2, 5 and 10 nM to form SERS probes-agarose solutions. Subsequently, the above solution was separately transferred into the wells of the 96-well plate (100 μL for each well). After the solidification, SERS imaging of each agarose phantom was performed with a 633 nm laser and 1 s exposure time (100 μm step size, 5 × objective, about 20 min imaging time).

2.9. In vitro detection of the penetration depth of SERS probe

The penetration depth of the SERS probe was tested on the agarose phantoms. SERS probe (0.5 μL, 10 nM) was injected into the agarose phantoms using a microliter syringe at the depths of 0.5, 1.0, 1.5 and 2.0 mm. After the solidification, SERS imaging of each agarose phantom was performed with a 633 nm laser and 1 s exposure time (100 μm step size, 5 × objective, about 20 min imaging time).

2.10. Establishment of xenotransplanted breast tumor model

All animal experiments were carried out in the animal experiment center of Hainan Medical University following the experimental protocol approved by the Animal Protection Committee.

Female Balb/c nude mice (18–20 g, 6–8 weeks) were used to establish the xenotransplanted breast tumor model. In brief, the Balb/c mice were anesthetized through isoflurane under pathogen-free conditions. Then, the SK-BR-3 breast cancer cells (10^6 cells/mouse, in 50 μL PBS) were injected into the right axilla of the mice. Tumor growth continued for 21 days.

2.11. Therapeutic evaluation

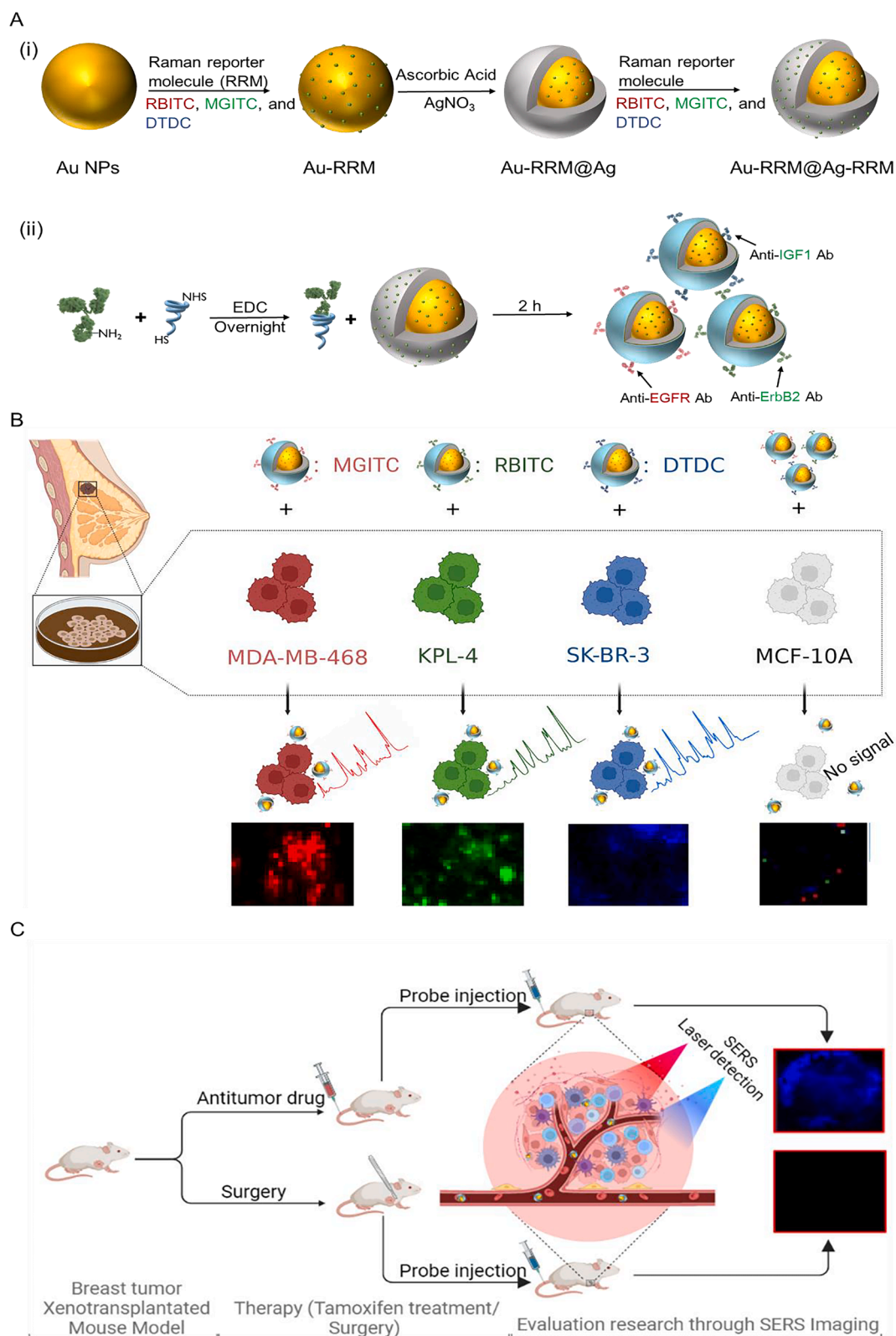
Breast tumor-bearing mice were intravenously injected with SERS probe solution (100 μL, 10 nM). After 12 h of circulation, the SERS imaging of in vivo breast tumor was obtained. In contrast, healthy mice were selected as the control group and injected with SERS probe (100 μL, 10 nM) intravenously. Then, the right axilla was exposed for SERS imaging at 12 h post-injection. The anticancer drug (tamoxifen, 25 μg/kg, 100 μL) was injected into the breast tumor-bearing mice by intravenous injection for 14 days, and the treatment was repeated at two-day intervals. Afterward, the SERS probe was intravenously injected for imaging breast tumors and important organs. In the surgery group, the macroscopic subcutaneous tumor tissue was completely resected, then, the SERS probe was intravenously injected for imaging to confirm the surgical removal efficiency. SERS imaging was performed using an inVia Qontor Raman microscope (Renishaw) equipped with a 633 nm laser. StreamLine high-speed acquisition mode (5 × objective) and an exposure time of 1 s was selected to obtain the SERS images. The SERS probe feature at 1646 cm⁻¹ was selected for pixel image processing. The total time of Raman mapping is about 30 to 45 min.

3. Results and discussion

3.1. Protocols of SERS application

As illustrated by previous research, the development and metastasis of the breast cancers are closely related to the specific biomarkers expressed on the surface of tumor cells and tumor microenvironment. In addition, the molecular phenotype affects the treatment responses and prognosis, which mainly depends on the specific biomarkers. Therefore, the detection of specific biomarkers has the great potential to be a useful method to simultaneously detect the molecular phenotype and evaluate the treatment efficacy. Numerous research focus on the single biomarker detection, however, the single biomarker cannot fully meet the requirement of clinical diagnosis and often causes false results due to lack of specificity (Table S1). Thus, the simultaneous detection of multiple biomarkers becomes the powerful tool to overcome the obstacle. In addition, the therapeutic efficacy after treatment plays an important role to improve the prognosis. Scheme 1 illustrates the fabrication of three different SERS probes and the application of SERS imaging to detect specific biomarkers expressed in breast cancer and normal cells and the therapeutic efficacy evaluation after chemotherapy and surgery treatment. In this study, three biomarkers including epidermal growth factor receptors (EGFR and ErbB2) and insulin-like growth factor 1 (IGF1) receptor were selected as the detection targets, which exhibited over-expression in MDA-MB-468, KPL-4 and SK-BR-3 human breast cancer cell lines, respectively. Simultaneously, these three proteins displayed ultralow expression in MCF-10A normal human breast cell line. Three types of SERS probes functionalized the Raman reporter molecules MGITC, RBITC and DTDC, respectively, were prepared as illustrated in Scheme 1A. To improve the conjugation efficiency and prevent aggregation of SERS probes, the antibodies were first mixed with HS-PEG-NHS at 1:1 M ratio. After incubating overnight at 4 °C, the complexes of functional PEG and antibodies were then immobilized on the silver shell surface of Raman reporter embedded Au@Ag nanoparticles. Scheme 1B illustrates the phenotypic biomarker detection using the specific SERS probes toward the cancer cell lines and normal breast cell line. Here, EGFR, ErbB2 and IGF1 biomarkers on the cell surface could be detected through SERS imaging. Then, the expression of each protein could be quantified according to the average SERS intensity from the SERS imaging.

Benefited from the excellent performance of SERS probes, the SERS probes were expanded to the therapeutic efficacy using the breast tumor xenotransplanted nude mice models that constructed using KPL-4 cells. After antitumor drug tamoxifen treatment and surgery removing the solid tumor, the solution of SERS probe was intravenously injected to



Scheme 1. (A) Schematic illustrations (i) for the fabrication of three different Raman reporter-adsorbed Au-Ag core-shell nanoparticles and the conjugation of PEGylated antibodies on the surface of the above Au-Ag core-shell nanoparticles. (B) Detection of phenotypic biomarkers on cell surface membranes via SERS imaging. (C) The evaluation of after antitumor drug and surgery treatment through SERS imaging. The illustrations (B and C) were created with the help of [BioRender.com](https://www.biorender.com).

image the tumor change before and after treatment via SERS imaging. The therapeutic efficacy was further confirmed by H&E and Masson staining.

3.2. Optimization of SERS-active Au@Ag core-shell nanoparticles

In this work, Au@Ag core-shell nanoparticles were selected as SERS active substrate and MGITC, RBITC and DTDC molecules as Raman reporters were adsorbed on the surface of SERS substrate. Here, MGITC was used as the selected Raman reporter to test the performance of SERS substrate. MGITC molecules were attached on the surface of 40 nm gold nanoparticles. Subsequently, the silver shell coating AuNPs was fabricated through the reduction of silver nitrate by ascorbic acid. In addition, the second layer of MGITC was functionalized on the surface of the silver shell to further enhance the SERS signal intensity. The SERS signal is closely related to the silver shell thickness, which can be controlled by changing the volume of AgNO_3 and AA. As the silver shell increasing, the red color gradually changed to light yellow (Fig. 1B). With the increased volume of AgNO_3 and AA from 20 μL to 80 μL , the characterized absorbance peaks exhibited blue shift with the increased addition of silver-staining solution, corresponding to the shell thickness from 2 nm to 5 nm (Fig. 1C). It was found that the SERS signal intensity at 1616 cm^{-1} gradually increased with the addition of silver-staining solution, up to 60 μL , but decreased when the volume reached to 80 μL (Fig. 1D). High-angle annular dark field-scanning/transmission electron microscopy (HAADF-STEM) was used to further confirm the formation of the silver shell, which showed clear core-shell nanostructure. Furthermore, energy dispersive spectra (EDS) were procured for elemental analysis of Au@Ag core-shell nanoparticles.

To select the optimized core-shell nanoparticle types for fabrication of SERS probes, SERS signals for AuNPs-MGITC, AuNPs-MGITC@Ag, AuNPs@Ag-MGITC and AuNPs-MGITC@Ag-MGITC were compared in Fig. 2A. As expected, AuNPs-MGITC@Ag-MGITC exhibited much stronger SERS signal intensity at 1616 cm^{-1} than other types of nanoparticles under the same test conditions, which was attributed to the more Raman reporter immobilization on the surface of Au core and Ag shell. Therefore, the AuNPs-MGITC@Ag-MGITC type of nanoparticles

was used for further bioconjugation with specific antibodies on the surface of the silver shell. UV-vis spectra displayed a slight red shift from 502 nm to 518 nm as shown in Fig. 2B. After antibodies conjugation, DLS data indicated a slight increase of the probe size compared to Au@Ag core-shell nanoparticles (Fig. 2C). From SERS spectra, no significant changes were observed before and after antibodies conjugation (Fig. 2D), demonstrating the conjugation could not significantly affect the SERS signals. An important factor in the SERS probes is to maintain their stability in the biological environment, SERS signal intensity at 1616 cm^{-1} was investigated within 120 min in fetal bovine serum (FBS). No significant changes could be found, indicating the good stability in the biological milieu (Fig. 2E). Fig. 2F exhibited TEM image of SERS probes, from which diameters of the probes were estimated to be 75 nm. In addition, the properties of different types of SERS probes using RBITC and DTDC were tested under the same conditions, respectively (Figs. S1 and S2).

3.3. Western blot analysis

To confirm the overexpression of EGFR, ErbB2 and IGF1 proteins on the surface of MDA-MB-468, KPL-4, SK-BR-3 breast cancer cells and MCF-10A normal breast cells, respectively, a western blot analysis was performed as illustrated in Fig. 3A. As expected, MDA-MB-468 cells expressed a high level of EGFR than other cells, and KPL-4 overexpressed levels of ErbB2, and SK-BR-3 showed the highest level of IGF1, while MCF-10A cells expressed ultralow levels of three biomarkers. Fig. 3B compares western blot data for the four cell lines.

3.4. Cytotoxicity test and optimization of incubation time of cancer cells and SERS probes

CCK-8 assay was performed to assess the cytotoxicity of SERS probes to the living cells. The three SERS probes were incubated with four cell lines, respectively, and no significant cytotoxicity could be detected even at SERS probes concentrations as high as 10 nM, demonstrating the low cytotoxicity of three SERS probes (Fig. S3).

During the experiments, interestingly, we found that the SERS

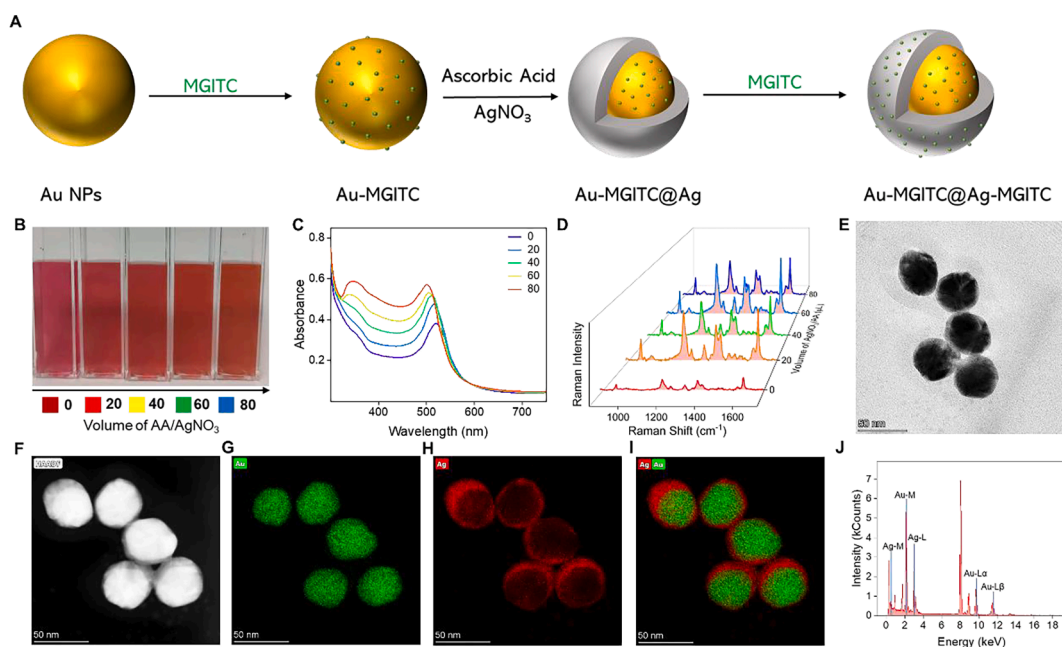


Fig. 1. Preparation and characterization of Au@Ag core-shell nanoparticles. (A) The preparation process of Raman reporter-labeled Au@Ag nanoparticles. (B) Photography for various Ag shell thicknesses. (C) UV-vis spectra of Au@Ag core-shell nanoparticles. (D) SERS signal intensity at 1616 cm^{-1} for different volumes of silver nitrate and ascorbic acid solution. (E) TEM image of Au@Ag nanoparticles for the volume of silver staining solution at 60 μL . (F-J) HAADF-STEM and EDS elemental maps of Au@Ag nanoparticles display clear core-shell geometry.

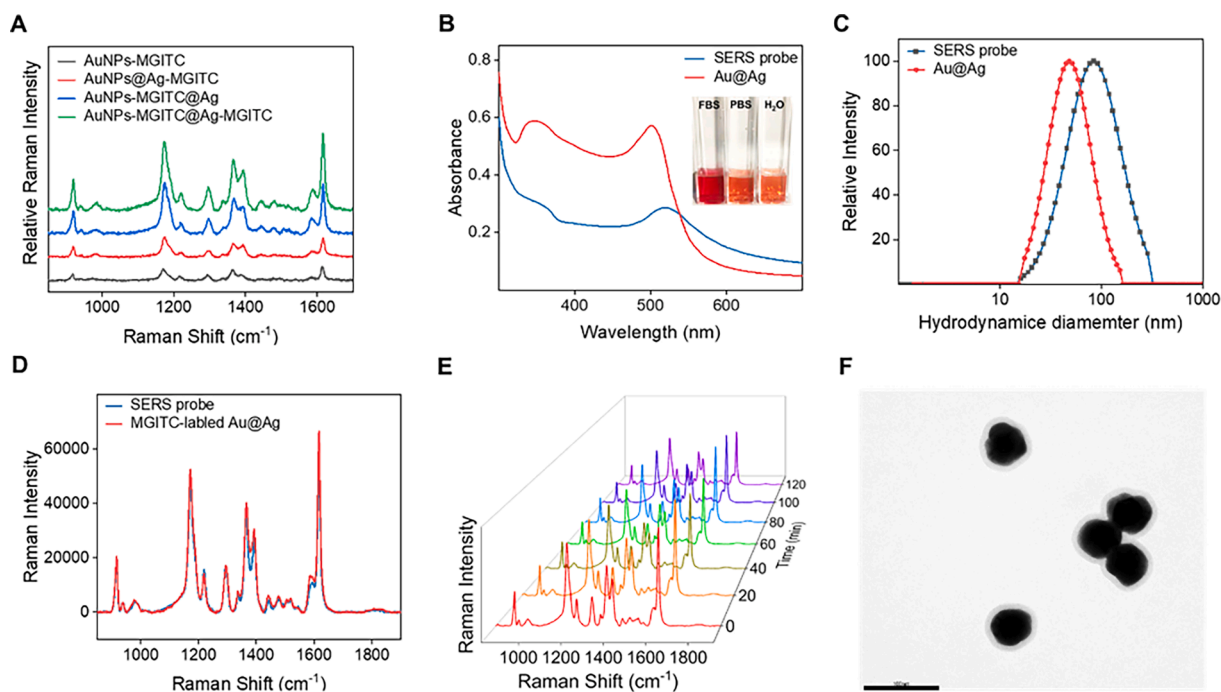


Fig. 2. (A) Selection of different types of SERS probes. Characterization of SERS probes: (B) UV-vis spectra, insert: photographs of SERS probes in FBS, PBS and H₂O (C) DLS distributions, (D) SERS spectra of nanoparticles before (red) and after (black) antibody conjugation, (E) Stability test of SERS signal intensity of SERS probes during incubation in 100 % FBS for 2 h, (F) TEM image of SERS probe. The scale bar is 100 nm.

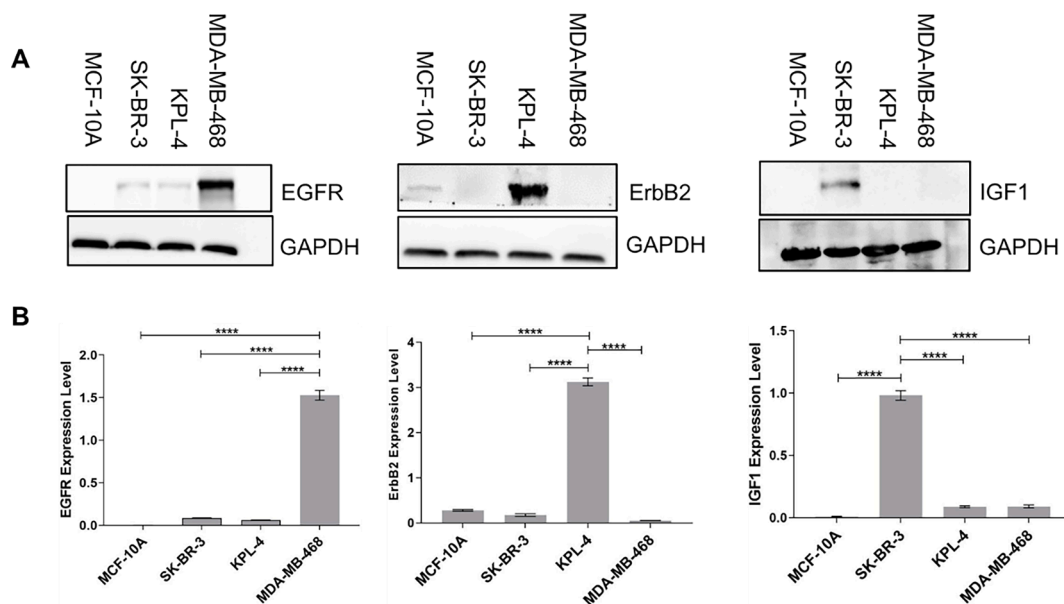


Fig. 3. (A) Western blot analysis for EGFR, ErbB2 and IGF1 biomarkers expressed in MD-MDA-468, KPL-4 and SK-BR-3 breast cancer cells and MCF-10A normal breast cells, respectively, GAPDH used as the internal standard. (B) Densitometric analysis of A, the optical density of biomarkers normalized against GAPDH ($n = 3$, mean \pm S. E. M., **** $P < 0.0001$). Statistical analysis was performed using a one-way ANOVA test.

imaging quality was closely related to the incubation time between cancer cells and SERS probes. To optimize the incubation time, three breast cancer cells were incubated with the corresponding SERS probes for 0, 1, 2, 5 h, then SERS imaging was obtained under the same conditions. The expression levels of EGFR, ErbB2 and IGF1 were indicated as red, green and blue colors, respectively, which corresponded to the typical peaks of SERS probes at 1616 cm^{-1} (MGITC), 1646 cm^{-1} (RBITC) and 1133 cm^{-1} (DTDC), respectively (Fig. S4). According to the SERS signal intensity after incubation for 2 h, the SERS signal intensity could reach an excellent level. Therefore, 2 h was selected as the optimized

incubation time for further cell imaging. To confirm the application of single-cell diagnosis in this research, MDA-MB-468, KPL-4 and SK-BR-3 cells were selected to test the heterogeneity, respectively. Three random cells in the same visual field were imaged and the mean SERS signal intensity for each cell was analyzed. The coefficient of variation for each cell line was calculated to be less than 10 %, which could meet the standard for single-cell diagnosis (Fig. S5).

3.5. Phenotypic types of breast cancer cells

The detection of phenotypic types depends on the specific recognition of SERS probes toward the biomarkers overexpressed on the surface of cancer cells. The SERS signals of typical peak of Raman reporter molecules were selected as signatures of specific biomarkers, and SERS imaging could be obtained for the analysis of three biomarkers as illustrated in Fig. 4.

The expressions of three biomarkers in one normal breast cell line MCF-10A and three breast cancer cell lines MDA-MB-468, KPL-4 and SK-BR-3 were tested by SERS imaging, which was performed after 2 h of incubation with corresponding antibody-conjugated SERS probes. Fig. 4 exhibited the SERS-mapping images of EGFR (MGITC), ErbB2 (RBITC) and IGF-1 (DTDC), displayed in red, green and blue colors for the above four cell lines. Only MDA-MB-468, KPL-4 and SK-BR-3 cells demonstrated high expression levels of EGFR, ErbB2 and IGF-1, respectively. Simultaneously, MCF-10A showed an ultralow expression level for the three biomarker proteins. These results were consistent with the western blot data in Fig. 3. The overlay images described overlays of representative colors for the distribution of the three biomarkers of KPL-4 cell (left) and MCF-10A cell (right). As illustrated in these figures, detailed local distribution of multiple biomarkers expressed on specific cancer cells and normal cells could be easily identified using the SERS-imaging technique, which has the potential to be used as a non-invasive method for the precise diagnosis of breast cancer in the molecular level.

3.6. Therapeutic efficacy evaluation

The performance of the SERS probe can greatly affect the detection limit and penetration depth of *in vivo* application. Before performing the *in vivo* test, the agarose phantom was used as soft tissue mimics to measure the signals of SERS probes with concentration range of 0–10

nM. As a result, the Raman detection threshold based on SERS imaging could be estimated as 1 nM at 1 s exposure time and $5 \times$ objective (Fig. S6A). Subsequently, the penetration depth was tested through SERS imaging of agarose phantom at increasing depths, which could reach about 2.0 mm (Fig. S6B). These results are sufficient for the detection of xenotransplanted breast tumors after chemotherapy with the anticancer drug tamoxifen and surgery, which is normally in the range of 1–2 mm depth.

Hereafter, the evaluation of therapeutic efficacy was assessed by using SERS imaging before and after treatment. The healthy mouse was selected as the negative control group (Group A) and mice bearing xenotransplanted breast tumors were divided into three groups without and with various treatments (Group B: tumor group without any treatment; Group C: tumor with anticancer drug tamoxifen treatment; Group D: tumor resection with standard surgery) as illustrated in Fig. 5. After intravenous injection with SERS probes targeting IGF1 for 12 h, the *in vivo* SERS imaging of tumor location was obtained, exhibiting low SERS signal intensity. Then, the mouse was sacrificed and major organs were excised and imaged *in vitro*, whereas only the liver and kidney displayed relatively high SERS signals. These results might be contributed to the metabolism of SERS probes in the liver and spleen. In contrast, the xenotransplanted tumor showed very high SERS signal intensities while major organs remained low signal intensities, indicating the active-targeting capability of SERS probes (Fig. 5B). After anticancer drug tamoxifen treatment for 15 days, the SERS signal-positive areas decreased compared to the tumor group, demonstrating its inhibition effect towards the breast tumor (Fig. 5C). As shown in Fig. 5D, mouse treated with standard surgery displayed almost no significant SERS signals, indicating the complete tumor elimination.

To further access the toxicity of SERS probes and therapeutic efficacy, the tumor (the skin tissue in healthy mice) and main organs (heart, liver, spleen, lung and kidney) of the mice in four groups were collected

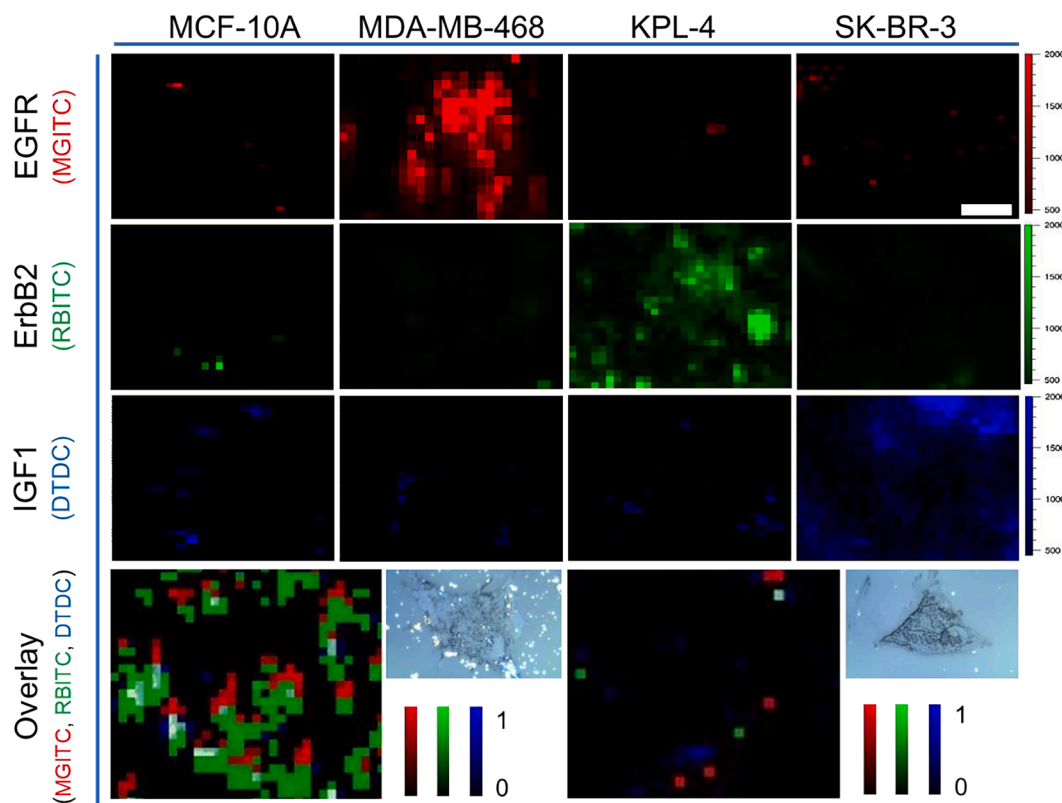


Fig. 4. SERS mapping images of triple biomarkers (EGFR, ErbB2 and IGF1) in MCF-10A, MDA-MB-468, KPL-4 and SK-BR-3 cancer cells after incubation with SERS probes for 2 h. Overlay of representative colors for the distribution of triple biomarkers in KPL-4 cell line (left) and MCF-10A cell line (right). Bright-field images of KPL-4 cell and MCF-10A cell are presented on the right side of SERS mapping images, respectively. The scale bar is 10 μ m.

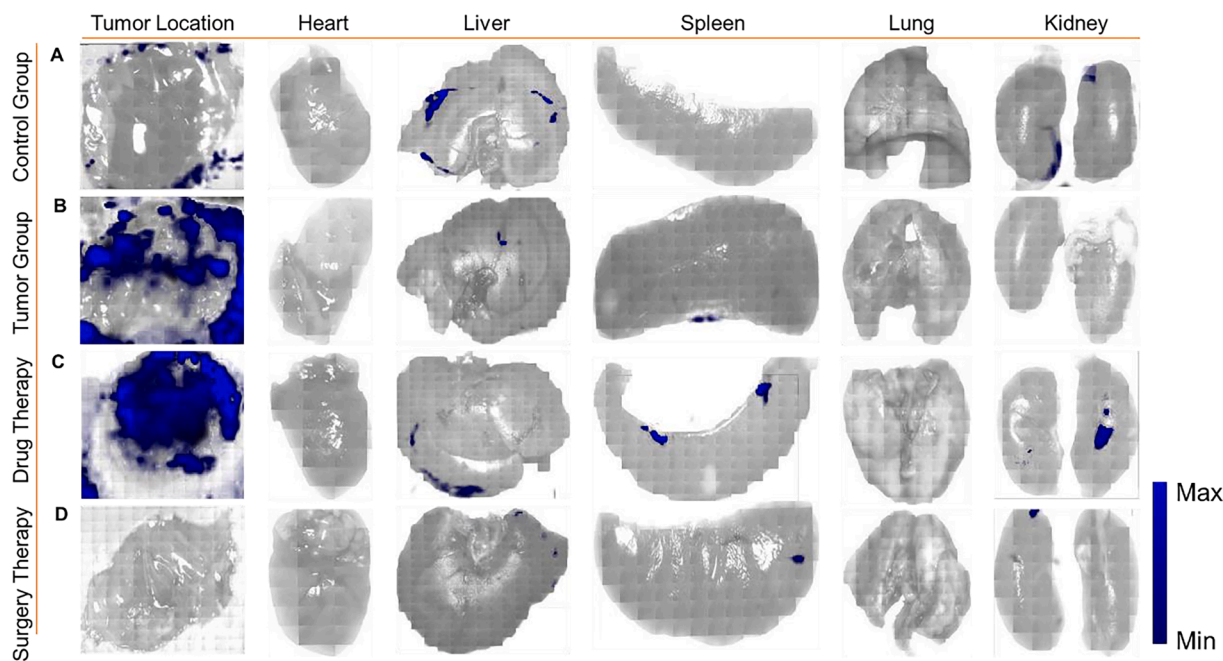


Fig. 5. The evaluation of before and after treatment towards the tumors based on SERS imaging. All the SERS imaging of tumors (the skin tissue in healthy mice) was performed *in vivo* while the main organs were imaged *in vitro*. (A) Control group: SERS imaging of right axilla of healthy nude mice and organs. (B) Tumor group: SERS imaging of breast tumor and organs without any treatment. (C) Drug therapy group: SERS imaging of breast tumor and organs after tamoxifen treatment for 15 days. (D) Surgery therapy group: SERS imaging of breast tumor and organs after surgery.

for H&E and Masson staining (Fig. S7). In the control group, no obvious toxicity of harvest organs was illustrated after intravenous injection of SERS probes, suggesting the biosafety of the SERS imaging technique. In the tumor group, the main organs exhibited increased infiltration of inflammatory cells, cell edema and muscle fibrosis. The liver displayed cell necrosis and more mononucleosis in the portal vein area. The spleen showed neutrophils in the red pulp with focal necrosis. Renal interstitial inflammatory cells were infiltrated, and tubular epithelial cells were irregularly arranged. Compared with the tumor group, the pathological tissue sections exhibited a lower degree of tissue damage in each organ in the anticancer drug treatment and surgery groups.

4. Conclusion

In summary, we explored a SERS imaging technique using highly sensitive SERS probes for precisely phenotypic diagnosis at the single cell level and therapeutic evaluation after chemotherapy and surgical treatment. The Au@Ag core-shell nanoparticles embedding double-layer Raman reporters were conjugated with specific antibodies on the surface of the Ag shell to fabricate the SERS probes for the highly sensitive multiplex detection of three phenotypic biomarkers expressed on the surface of breast cancer cell lines. The results demonstrated that the expression level of three biomarkers as well as cancer cell phenotypes could be distinguished specially based on SERS imaging. Furthermore, the therapeutic efficacy after chemotherapy and surgical treatment was evaluated through SERS imaging. We believe that the precisely phenotypic diagnosis and therapeutic evaluation of breast cancers would broaden SERS-based imaging toward a wide range of *in vivo* biomedical applications.

Declaration of Competing Interest

The authors declare that they have no known competing financial interests or personal relationships that could have appeared to influence the work reported in this paper.

Data availability

No data was used for the research described in the article.

Acknowledgments

This work was supported by the National Natural Science Foundation of China (Nos. 21864011, 22264013 and 21904030), Hainan Provincial Natural Science Foundation of China (Nos. 2019RC220), Hainan Key Research and Development Project (Grant ZDYF2020133), Natural Science Research Talent Project of Hainan Medical University (Grant JBGS202101), Hainan Province Clinical Medical Center (2021), Project for Functional Materials and Molecular Imaging Science Innovation Group of Hainan Medical University, Nanhai Young-Talent Program of Hainan (20202007).

Appendix A. Supplementary data

Supplementary data to this article can be found online at <https://doi.org/10.1016/j.cej.2023.141502>.

References

- [1] R.L. Siegel, K.D. Miller, H.E. Fuchs, A. Jemal DVM, Cancer statistics, 2022, CA: Cancer J. Clin. 72 (2022) 7–33.
- [2] A.G. Rivenbark, S.M. O'Connor, W.B. Coleman, Molecular and cellular heterogeneity in breast cancer: challenges for personalized medicine, *Am. J. Pathol.* 183 (4) (2013) 1113–1124.
- [3] D. Zardavas, A. Irrthum, C. Swanton, M. Piccart, Clinical management of breast cancer heterogeneity, *Nat. Rev. Clin. Oncol.* 12 (7) (2015) 381–394.
- [4] N. Radošević-Robin, P. Selenica, Y. Zhu, H.H. Won, M.F. Berger, L. Ferrando, E. Cocco, M. Privat, F. Ponelle-Chachuat, C. Abrial, J.M. Nabholz, F. Penault-Llorca, J.S. Reis-Filho, M. Scaltriti, Recurrence biomarkers of triple negative breast cancer treated with neoadjuvant chemotherapy and anti-EGFR antibodies, *NPJ Breast Cancer* 7 (1) (2021) 124.
- [5] B. He, L. Bergenstråhle, L. Stenbeck, A. Abid, A. Andersson, Å. Borg, J. Maaskola, J. Lundeberg, J. Zou, Integrating spatial gene expression and breast tumour morphology via deep learning, *Nat. Biomed. Eng.* 4 (8) (2020) 827–834.
- [6] M.J. Duffy, J. Crown, A personalized approach to cancer treatment: how biomarkers can help, *Clin. Chem.* 54 (11) (2008) 1770–1779.

- [7] H.W. Jackson, J.R. Fischer, V.R.T. Zanotelli, H.R. Ali, R. Mechera, S.D. Soysal, H. Moch, S. Muenst, Z. Varga, W.P. Weber, B. Bodenmiller, The single-cell pathology landscape of breast cancer, *Nature* 578 (7796) (2020) 615–620.
- [8] S.Y. Chae, S.Y. Ahn, S.B. Kim, S. Han, S.H. Lee, S.J. Oh, S.J. Lee, H.J. Kim, J.W. Lee, B.H. Son, J. Kim, J.H. Ahn, K.H. Jung, J.E. Kim, S.Y. Kim, W.J. Choi, H.J. Shin, G. Gong, H.S. Lee, J.B. Lee, H.M. Moon, Diagnostic accuracy and safety of ^{18}F -fluoro-17 β -oestradiol PET-CT for the assessment of oestrogen receptor status in recurrent or metastatic lesions in patients with breast cancer: a prospective cohort study, *Lancet Oncol.* 20 (4) (2019) 546–555.
- [9] Z. Liu, Z. Li, R. Zhang, X. Zhou, L. Li, K. Sun, Z. Tang, H. Jiang, H. Li, Q. Xiong, Y. Ding, X. Zhao, K. Wang, Z. Liu, J. Tian, Radiomics of Multiparametric MRI for pretreatment prediction of pathologic complete response to neoadjuvant chemotherapy in breast cancer: a multicenter study, *Clin. Cancer Res.* 25 (12) (2019) 3538–3547.
- [10] J. Ouyang, L. Sun, Z. Zeng, C. Zeng, F. Zeng, S. Wu, Nanoaggregate probe for breast cancer metastasis through multispectral optoacoustic tomography and aggregation-induced NIR-I/II fluorescence imaging, *Angew. Chem. Int. Ed.* 132 (25) (2020) 10197–10207.
- [11] X. Hao, C. Li, Y. Zhang, H. Wang, G. Chen, M. Wang, Q. Wang, Programmable chemotherapy and immunotherapy against breast cancer guided by multiplexed fluorescence imaging in the second near-infrared window, *Adv. Mater.* 30 (51) (2018) 1804437.
- [12] Y. Cao, Y. Dai, H. Chen, Y. Tang, X. Chen, Y. Wang, J. Zhao, X. Zhu, Integration of fluorescence imaging and electrochemical biosensing for both qualitative location and quantitative detection of cancer cells, *Biosens. Bioelectron.* 130 (2019) 132–138.
- [13] Y. Wen, V.X. Truong, M. Li, Real-time intraoperative surface-enhanced Raman spectroscopy-guided thermosurgical eradication of residual microtumors in orthotopic breast cancer, *Nano Lett.* 21 (7) (2021) 3066–3074.
- [14] S. Lin, Z. Cheng, Q. Li, R. Wang, F. Yu, Toward sensitive and reliable surface-enhanced Raman scattering imaging: from rational design to biomedical applications, *ACS Sens.* 6 (11) (2021) 3912–3932.
- [15] N.C. Lindquist, C.D.L. de Albuquerque, R.G. Sobral-Filho, I. Paci, A.G. Brolo, *Nat. Nanotech.* 14 (10) (2019) 981–987.
- [16] C. Qiu, Z. Cheng, C. Lv, R. Wang, F. Yu, Development of bioorthogonal SERS imaging probe in biological and biomedical applications, *Chin. Chem. Lett.* 32 (8) (2021) 2369–2379.
- [17] A. Kapara, V. Brunton, D. Graham, K. Faulds, Investigation of cellular uptake mechanism of functionalised gold nanoparticles into breast cancer using SERS, *Chem. Sci.* 11 (22) (2020) 5819–5829.
- [18] F. Nicolson, A. Ali, M.F. Kircher, S. Pal, DNA nanostructures and DNA-functionalized nanoparticles for cancer theranostics, *Adv. Sci.* 7 (23) (2020) 2001669.
- [19] Q. Li, X. Ge, J. Ye, Z. Li, L. Su, Y. Wu, H. Yang, J. Song, Dual ratiometric SERS and photoacoustic core-satellite nanoprobe for quantitatively visualizing hydrogen peroxide in inflammation and cancer, *Angew. Chem. Int. Ed.* 60 (13) (2021) 7323–7332.
- [20] Y. Qiu, Y. Zhang, M. Li, G. Chen, C. Fan, K. Cui, J.B. Wan, A. Han, J. Ye, Z. Xiao, Intraoperative detection and eradication of residual microtumors with gap-enhanced Raman tags, *ACS Nano* 12 (8) (2018) 7974–7985.
- [21] J. Yang, T. Wang, L. Zhao, V.K. Rajasekhar, S. Joshi, C. Andreou, S. Pal, H. Hsu, H. Zhang, I.J. Cohen, R. Huang, R.C. Hendrickson, M.M. Miele, W. Pei, M. B. Brendel, J.H. Healey, G. Chiosis, M.F. Kircher, Gold/alpha-lactalbumin nanoprobe for the imaging and treatment of breast cancer, *Nat. Biomed. Eng.* 4 (7) (2020) 686–703.
- [22] S. Lee, H. Chon, J. Lee, J. Ko, B.H. Chung, D.W. Lim, J. Choo, Rapid and sensitive phenotypic marker detection on breast cancer cells using surface-enhanced Raman scattering (SERS) imaging, *Biosens. Bioelectron.* 51 (2014) 238–243.
- [23] Z. Zhang, J. Wang, K.B. Shanmugasundaram, B. Yeo, A. Möller, A. Wuethrich, L. L. Lin, M. Trau, Tracking drug-induced epithelial-mesenchymal transition in breast cancer by a microfluidic surface-enhanced Raman spectroscopy immunoassay, *Small* 16 (2020) 1905614.
- [24] J. Wang, D. Liang, J. Feng, X. Tang, Multicolor cocktail for breast cancer multiplex phenotype targeting and diagnosis using bioorthogonal surface-enhanced Raman scattering nanoprobe, *Anal. Chem.* 91 (17) (2019) 11045–11054.
- [25] K. Oliveira, A. Teixeira, J.M. Fernandes, C. Lopes, A. Chácharo, P. Piairo, L. Wu, L. Rodríguez-Lorenzo, L. Diéguez, S. Abalde-Cela, Multiplex SERS phenotyping of single cancer cells in microdroplets, *Adv. Opt. Mater.* (2022) 2201500.
- [26] R. Wang, H. Chon, S. Lee, Z. Cheng, S.H. Hong, Y.H. Yoon, J. Choo, Highly sensitive detection of hormone estradiol E2 using surface-enhanced Raman scattering based immunoassays for the clinical diagnosis of precocious puberty, *ACS Appl. Mater. Inter.* 8 (17) (2016) 10665–10672.
- [27] E.A. Kwizera, R. O'Connor, V. Vinduska, M. Williams, E.R. Butch, S.E. Snyder, X. Chen, X. Huang, Molecular detection and analysis of exosomes using surface-enhanced Raman scattering gold nanorods and a miniaturized device, *Theranostics* 8 (10) (2018) 2722–2738.
- [28] N.G. Bastús, J. Comenge, V. Puntes, Kinetically controlled seeded growth synthesis of citrate-stabilized gold nanoparticles of up to 200 nm: size focusing versus Ostwald ripening, *Langmuir* 27 (17) (2011) 11098–11105.